scientific reports

Check for updates

OPEN

Aquaporin 1 aggravates lipopolysaccharide-induced macrophage polarization and pyroptosis

Zhuman Wen & Abduxukur Ablimit✉

Acute respiratory infections (ARIs) are associated with high mortality and morbidity. Acute lung injury (ALI) is caused by the activation of immune cells during ARIs caused by viruses such as SARS-CoV-2. Aquaporin 1 (AQP1) is distributed in a variety of immune cells and is related to the occurrence of ALI, but the mechanism is not clear. A reference map of human single cells was used to identify macrophages in COVID-19 patients at the single-cell level. "FindMarkers" was used to analyze differentially expressed genes (DEGs), and "clusterProfiler" was used to analyze the functions of the DEGs. An M1 macrophage polarization model was established with lipopolysaccharide (LPS) in vitro, and the relationships among AQP1, pyroptosis and M1 polarization were examined by using an AQP1 inhibitor. Transcriptome sequencing and RT-qPCR were used to examine the molecular mechanism by which AQP1 regulates macrophage polarization and pyroptosis. Antigen presentation, M1 polarization, migration and phagocytosis are abnormal in SARS-CoV-2-infected macrophages, which is related to the high expression of AQP1. An M1 polarization model of macrophages was constructed in vitro, and an AQP1 inhibitor was used to examine whether AQP1 could promote M1 polarization and pyroptosis in response to LPS. Transcriptome and cell experiments showed that this effect was related to a decrease in chemokines caused by AQP1 deficiency. AQP1 participates in M1 polarization and pyroptosis in macrophages by increasing the levels of chemokines induced by LPS, which provides new insights for the diagnosis and treatment of ALI.

Keywords Acute lung injury, Macrophages, Cell polarization, Pyroptosis, Chemokine

Acute respiratory infections (ARIs) are diseases with high mortality and morbidity[1]. According to the WHO, ARIs are the fourth leading cause of death in the world, and acute lower respiratory infections, including pneumonia and bronchitis, have become the main causes of infant death. COVID-19 was first reported at the end of 2019 and quickly became a global public health issue[2]. The data showed that the early symptoms of COVID-19 patients were fever and dry cough, and severe cases could involve acute lung injury (ALI) or acute respiratory distress syndrome (ARDS)[3]. At present, the SARS-CoV-2 S protein invades many kinds of cells via the ACE2 receptor, thereby destroying the epithelial-endothelial barrier and causing abnormal oxygen transmission[4]. Viral infection causes excessive activation of immune cells, including macrophages and monocytes, and exacerbates ALI[5]. Macrophages are highly heterogeneous and polarize into two phenotypes under different conditions. M2 macrophages have anti-inflammatory properties and promote the occurrence of tissue fibrosis[6]. During the acute exudation phase of ALI/ARDS, persistent M1 macrophage polarization can result in the release of tumor necrosis factor α (TNF-α), nitric oxide and reactive oxygen species, thereby inducing severe inflammatory reactions[7]. Water channels were first shown to control the entry and exit of water in cells. Recently, it was reported that aquaporin 1 (AQP1) is highly expressed during ALI induced by ischemia/reperfusion[8], but the molecular mechanism has not been determined. In addition, inhibiting pyroptosis mediated by NLRP3 can alleviate ALI induced by lipopolysaccharide (LPS)[9]. Therefore, there is an urgent need to clarify the relationships among AQP1, macrophage polarization and pyroptosis, which will provide a new understanding of the pathological mechanism and treatment of ALI.

This study examined the role of AQP1 in promoting M1 macrophage polarization by using single-cell data from patients with severe COVID-19. An M1 macrophage polarization model was constructed in vitro, and

Department of Histology and Embryology, Basic Medical College, Xinjiang Medical University, Urumqi, China. ✉email: 806613359@qq.com

AQP1 inhibitors were used to examine the effects of AQP1 on M1 polarization and pyroptosis. Transcriptome sequencing revealed that AQP1 inhibitors regulated the molecular mechanism of pyroptosis and macrophage polarization by inhibiting the expression of chemokines. In addition, cell experiments revealed that high expression of AQP1 was related to macrophage migration/phagocytosis. In summary, this study comprehensively analyzed the biological role of AQP1, which can provide a new perspective on the pathological mechanism and treatment of ALI.

Methods

Data acquisition and standardization

The GSE171524 dataset[10], which included 7 normal individuals and 20 patients, and the GSE171668 dataset[11], which included 48 patients, were collected. Single-cell objects were constructed by the "Seurat" algorithm[12], and qualified single-cell data were obtained with the thresholds of a gene expression number greater than 50 and a mitochondrial gene ratio less than 20%. The normalization factor was set to 10,000 to standardize the data, and 5000 highly variable genes were identified via the "vst" method. After normalization, principal component analysis was used for dimensionality reduction clustering, and the cells were grouped at a resolution of 0.6. Finally, according to the marker genes of the cell clusters, "singleR" was used to annotate cell types based on the human cell atlas. For transcriptome sequencing, the FPKM data were logarithmically normalized.

Differentially expressed genes (DEGs) and enrichment analysis

Based on the single-cell data, the macrophages were regrouped according to gene expression. For example, macrophages with AQP1 expression and macrophages without AQP1 expression were separated, and similar methods were applied to TLR2, TLR4 and CD86. The Wilcoxon rank sum test and the "FindMarkers" algorithm[13] were used to analyze DEGs in cells with a gene expression ratio greater than 10%. According to the transcriptome sequencing results, DEGs were analyzed using "limma"[14]. The "clusterProfiler"[15] package was used for Gene Ontology (GO) and Kyoto Encyclopedia of Genes and Genomes (KEGG) analyses of DEGs. The activation or inhibition status of the terms was evaluated by calculating the Z score, and the "forcats" package was used to summarize the enrichment results for the different groups.

Identification of overlapping genes and construction of a protein−protein interaction network

A Venn diagram was used to visualize the overlapping DEGs. The STRING database[16] was used to examine the interactions among DEGs. The MCODE algorithm[17] in Cytoscape was used to investigate the important modules of the protein−protein interaction network.

Hub gene recognition and correlation analysis

Six algorithms (MCC, MNC, EPC, degree, radiality, and closeness) were used to identify the top 30 DEGs. The overlapping genes identified by all six algorithms were considered hub genes. The Pearson method was used to analyze the correlation between the expression levels of the hub genes and genes related to pyroptosis.

Cell culture and treatments

The MH-S mouse alveolar macrophage line (Procell, Wuhan, China) was partially adherent and partially suspended. After be retrieved from liquid nitrogen, MH-S cells were rapidly revived, placed in a Petri dish with complete culture medium (Procell, Wuhan, China), and incubated in a constant temperature incubator at 37 °C with 5% CO_2. Once the MH-S cells reached 70% to 80% confluence, the medium was removed, and the cells were washed with PBS (HyClone, Utah, USA), digested with 0.25% trypsin (HyClone, Utah, USA), and centrifuged at 1000 r/min at room temperature for 5 min. The supernatant was discarded, and the cells were resuspended and subcultured. For western blot and RT-qPCR analyses, MH-S cells were inoculated onto a 6-well plate at a density of 2×10^6 cells/well.

Construction of the M1 macrophage polarization model

MH-S cells in the logarithmic growth phase were selected, the supernatant was discarded, and the cells were washed twice with PBS, digested with trypsin and centrifuged. The centrifuged cells were suspended in complete culture medium, the cell concentration was adjusted to 5×10^5 cells/mL, and the cells were seeded in 6-well plates at 3×10^5 cells/well. After the cells had adhered to the wells for 12 h, different concentrations of LPS (1 μg/mL, 5 μg/mL or 10 μg/mL) were added, and the cells were incubated for 12 h or 24 h to establish the M1 macrophage model.

AQP1 protein inhibitor and agonist screening

MH-S cells in the logarithmic growth phase were selected and seeded in 6-well plates at 3×10^5 cells/well. After 12 h, the cells were treated with LPS and AQP1 agonists or inhibitors, including different concentrations of MG132 (3 μM, 10 μM, and 30 μM), merbromin (50 μM, 100 μM, and 150 μM) and TEA (3 μM, 30 μM, and 100 μM). After 12 h, the cells were collected, and protein was extracted for verification.

Evaluation of macrophage migration

On the back of a 6-well plate, parallel horizontal lines were drawn, and approximately 3×10^6 cells were inoculated into each well. The plate was then placed in an incubator for 12 h. Subsequently, additional horizontal lines were drawn vertically on the back of the plate using a 10 μL pipette. Next, the cells were washed with PBS 2–3 times, and the medium was replaced with fresh serum-free medium. The plate was returned to the incubator

for an additional 12 h. Then, the cells were observed and photographed under a microscope. ImageJ software was used to calculate the average intercellular distance between 6–8 randomly selected horizontal lines. For the transwell chamber experiment, cells were inoculated at a density of 5×10^5 cells/well. In the lower layer of the chamber, 800 μL of 1640 medium (Gibco, USA) containing 20% serum (Sigma, USA) was added, and the upper layer contained 100 μL of pretreated cells. After 12 h of incubation, the transwell chamber was removed and washed with PBS, and the cells were stained with crystal violet. The stained cells were then photographed under a microscope, and ImageJ was used to calculate the number of migrated cells.

Examination of macrophage phagocytosis

MH-S cells were inoculated into 12-well plates at a density of 1×10^6 cells per well. After the cells adhered to the wells, 1 μL of FITC-labeled fluorescent microspheres (Poly Sciences, Shanghai, China) was added to each well and incubated for 2 h at 37 °C. The culture supernatant was then aspirated, and 0.25% trypsin was added to digest the cells. The cells were collected, fixed with paraformaldehyde, and subjected to flow cytometry to assess the phagocytosis of fluorescent microspheres by MH-S cells. Additionally, cells subjected to the same pretreatment procedure were covered with Hoechst 33342 staining solution (Beyotime, Shanghai, China) and observed and photographed under an inverted fluorescence microscope.

Examination of chemokines and cytokines by RT-qPCR

Total RNA was extracted from MH-S cells using TRIzol reagent, and RNA purity and concentration were determined using a spectrophotometer. Subsequently, reverse transcription was performed using a reverse transcription kit (Thermo Fisher Scientific, USA), and RT-qPCR was performed according to the manufacturer's instructions (Qiagen, Germany) and the predetermined reaction time and temperature from the preliminary experiments. The procedure involved an initial activation step at 95 °C for 2 min, denaturation at 95 °C for 5 s, and annealing/stretching at 60 °C for 10 s for 40 cycles. The sequences of the primers used are listed in Table 1. Using GAPDH as the internal reference, the relative expression level of the target mRNA was analyzed using the $2^{(-\Delta\Delta Ct)}$ method. The described experiment was repeated three times.

Examination of protein expression levels

MH-S cells were assessed using a BCA protein assay kit. Equal amounts of protein were separated by 10% SDS-PAGE and subsequently transferred to a PVDF membrane. The membrane was then blocked with a PBS solution containing 5% skim milk at room temperature for 2 h. Next, the membranes were incubated with primary antibodies (AQP1, NLRP3, GSDMD, N-GSDMD, Caspase-1 and iNOS) overnight at 4 °C. After three washes with TBST solution, the PVDF membrane was incubated with the corresponding secondary antibody at room temperature for 2 h, followed by another three washes with TBST solution. The blot was developed using an

Name of prims	Sequences
Ccl2-F	GACCCCAAGAAGGAATGGGT
Ccl2-R	ACCTTAGGGCAGATGCAGTT
Ccl3-F	TCCCAGCCAGGTGTCATTTTCC
Ccl3-R	AGGCATTCAGTTCCAGGTCAGTG
Ccl4-F	CTCCAAGCCAGCTGTGGTAT
Ccl4-R	CCAGGGCTCACTGGGGTTAG
Cd40-F	AGTCGGCTTCTTCTCCAATCAGTC
Cd40-R	ACCTCCAAGTTCTTATCCTCACAGC
Cxcl10-F	CCCAAGTGCTGCCGTCATTTTC
Cxcl10-F	GCTTCCCTATGGCCCTCATTCTC
Icam1-F	GGAGACGCAGAGGACCTTAACAG
Icam1-R	GGCTTCACACTTCACAGTTACTTGG
Il-1α-F	AGATTCTGAAGAAGAGACGGCTGAG
Il-1α-R	GGTAGGTGTAAGGTGCTGATCTGG
Il-1β-F	TTCAGGCAGGCAGTATCACTCATTG
Il-1β-R	TGTCGTTGCTTGGTTCTCCTTGTAC
Nlrp3-F	CTCTGTTCACTGGCTGCGGATG
Nlrp3-R	TGGTCCTTTCCTCACGGTCTCC
Gsdmd-F	GGCAGCAGAGGCGATCTCATTC
Gsdmd-R	ACACATTCATGGAGGCACTGGAAC
Gapdh-F	CTCTGTTCACTGGCTGCGGATG
Gapdh-R	TGGTCCTTTCCTCACGGTCTCC

Table 1. Primer sequence information. *F* forward primer, *R* reverse primer.

enhanced chemiluminescence kit. ImageJ software was used to determine the gray values of the bands, and the ratio of the target protein to the internal reference, GAPDH, was used to calculate the relative protein expression.

ELISA assay

Levels of CCL4 in the macrophages were determined using commercially available ELISA kits (jianglai biology science and technology, Shanghai, China) according to the manufacture's instructions. The absorbance of each well recorded at 450 nm using a microplate reader.

Statistical analysis

The experimental values are presented as the mean ± SD. Statistical comparisons were performed using one-way analysis of variance and LSD-*t* test with GraphPad Prism version 9.0. Differences in values were considered statistically significant if the P values were < 0.05.

Results

The typical characteristics of severe COVID-19 are M1 macrophage polarization and pyroptosis

A total of 17,690 macrophages were identified through annotation of the single-cell transcriptome data from 27 lung tissue samples from the normal and severe COVID-19 groups (Fig. 1A). Analysis of the DEGs revealed significant differences between macrophages in the two groups, particularly in terms of abnormal antigen presentation processes, chemokine and cytokine production, migration, and phagocytosis (Fig. 1B). The expression of M1 markers (TLR2, TLR4, and CD86) in macrophages indicated a substantial increase in the proportion of M1 macrophages in patients with severe COVID-19 (Fig. 1C). The macrophages were further categorized into 14 subgroups (Fig. S1B). Notably, severe COVID-19 was predominantly associated with the 9th, 5th, and 3rd subgroups (Fig. 1D), and the cell groups coexpressing the three M1 markers were concentrated in these subgroups (Fig. 1E). A comparison of the functions of these three subgroups revealed increased reactivity to LPS and interferon-γ, which is indicative of M1 polarization. Moreover, M1 polarization was accompanied by cytokine production and enhanced phagocytic function (Fig. 1F). Furthermore, we regrouped the macrophage population based on M1 polarization markers. Analysis of the DEGs demonstrated that M1 polarization promoted macrophages hyperactivity (Fig. S1C). Functional enrichment analysis revealed that M1 polarization increased NLRP3 inflammasome formation, cytokine production, cell proliferation, and antigen presentation by macrophages (Fig. S1D). These findings suggest that the increase in M1 macrophages contributes to macrophage death and cytokine production during ARIs.

M1 macrophages are related to high expression of AQP1

To determine the relationship between M1 macrophages and AQP1, we selected the independent dataset GSE171668, which is exclusively composed of severe COVID-19 samples due to the limited number of macrophages in the GSE171524 dataset. A total of 89,892 macrophages were identified by cell annotation, resulting in 17 clusters (Fig. 2A). Macrophages expressing AQP1 exhibited increased M1 polarization and pyroptosis (Fig. 2B). DEG analysis further indicated a close association between AQP1 expression and macrophage activity (Fig. 2C). Functional analysis of the DEGs revealed significant similarities between AQP1 expression and M1 polarization markers (TLR2 and CD86) (Fig. 2D). These similarities included cell polarization, chemokine production, antigen processing and presentation, and immune pathway activation. Additionally, AQP1 colocalized with M1 polarization markers in macrophages (Fig. 2E,F). These findings strongly suggest the involvement of AQP1 in macrophage polarization toward the M1 phenotype during severe COVID-19.

High expression of AQP1 is related to pyroptosis

Given the evident correlation between AQP1 and M1 polarization, an in vitro model of macrophage polarization induced by LPS was established. At the protein level, the pyroptosis markers NLRP3 and GSDMD were significantly upregulated at 12 h (Fig. 3A–C). Additionally, the protein expression of AQP1 significantly increased in response to LPS ($P < 0.05$) (Fig. 3D). Furthermore, the mRNA and protein levels of pyroptosis markers decreased at 24 h (Fig. 3A–F), which coincided with a reduction in AQP1 protein expression. Consequently, 10 μg/mL LPS for 12 h was used to establish the M1 macrophage model.

Screening AQP1 protein inhibitors and agonists

According to published cell experiments involving AQP1 protein inhibitors and agonists, the agonist MG132 failed to significantly increase the protein expression of AQP1 ($P > 0.05$), and the inhibitor TEA did not decrease the expression of AQP1 (Fig. 4D). However, 150 μM merbromin significantly reduced the protein expression of AQP1. Moreover, merbromin decreased the expression of the pyroptosis marker NLRP3 without impacting the expression of GSDMD (Fig. 4A–D). To investigate whether merbromin could directly inhibit the AQP1 protein, LPS-induced macrophages were treated with various concentrations of merbromin. The results indicated a gradual decrease in the protein expression of AQP1 with increasing merbromin concentrations (Fig. 4E,F). Additionally, to further examine the interaction between merbromin and the AQP1 protein, molecular dynamics simulations were used to examine the binding stability of the proteins. The results demonstrated the stable binding of merbromin to the AQP1 protein (RMSD < 5), which likely involved various interaction forces (Fig. 4G,H).

AQP1 is involved in M1 polarization and pyroptosis in macrophages

To examine the biological effect of the AQP1 protein, we investigated the impact of an AQP1 inhibitor on LPS-induced cell polarization and pyroptosis. Compared with that in the LPS-only group, the AQP1 inhibitor

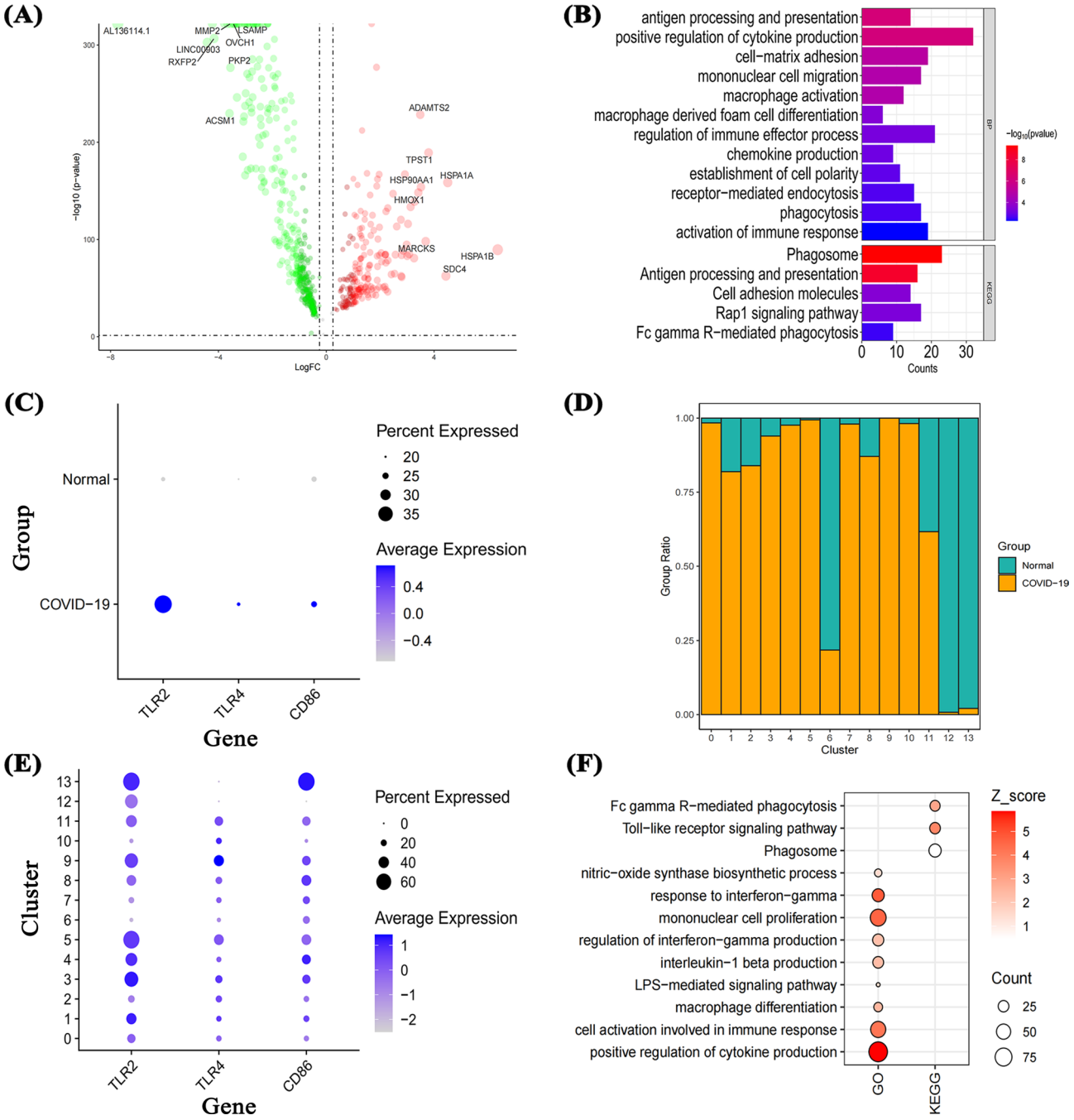

Figure 1. M1 macrophages are polarized during severe COVID-19. DEG analysis (**A**) and functional enrichment analysis (**B**) of macrophages in the severe COVID-19 group compared to the normal group. Polarization markers of M1 macrophages (**C**) and the proportions of different macrophage clusters in the two groups (**D**). The ratio and expression level of M1 markers in different macrophage clusters (**E**). Functional analysis of M1 macrophages compared with other macrophage clusters (**F**).

significantly inhibited the expression of iNOS ($P < 0.05$) (Fig. 5A,B), indicating a connection between the AQP1 protein and LPS-mediated macrophage polarization. Given that LPS-induced pyroptosis in macrophages was associated with an increase in AQP1 expression, blocking AQP1 significantly reduced the protein expression levels of pyroptosis markers, including NLRP3, GSDMD, and N-GSDMD ($P < 0.001$, $P < 0.01$, $P < 0.01$) (Fig. 5C,D,F), but not including Caspase-1 (Fig. 5E). This finding suggested that AQP1 plays a crucial role in connecting LPS and pyroptosis.

AQP1 is related to macrophage migration and phagocytosis

To determine the impact of AQP1 on macrophage function, scratch and transwell assays were performed. The results demonstrated that LPS significantly increased macrophage migration, and inhibiting AQP1 effectively

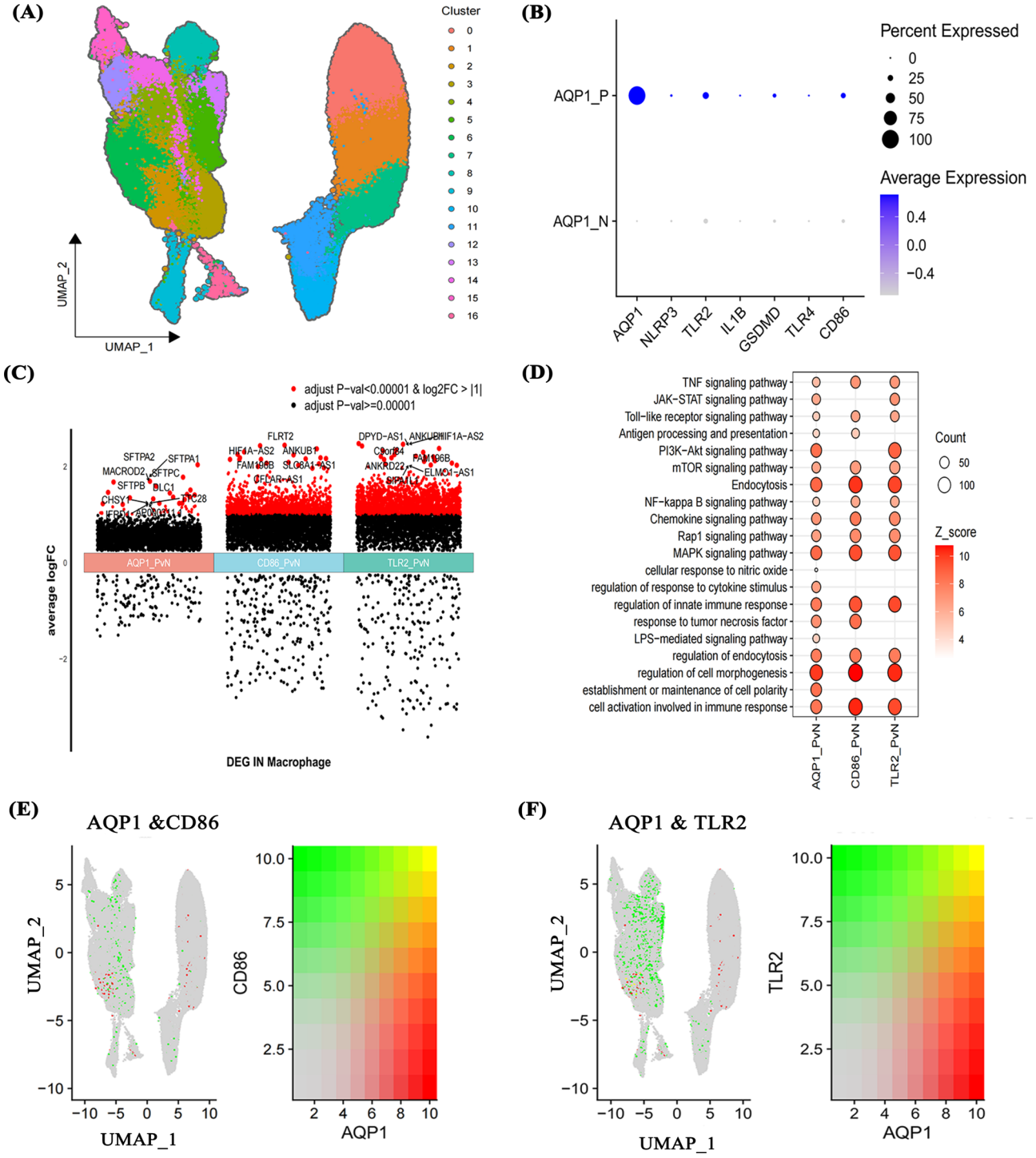

Figure 2. High expression of AQP1 is closely related to M1 macrophages. UMAP of the macrophage clusters (**A**). The expression of AQP1 is related to high expression of M1 macrophage markers (**B**), and the DEG (**C**) and functional enrichment analysis (**D**) results were compared with cells that did not express AQP1. AQP1 was coexpressed with M1 markers (CD86 and TLR2) in macrophages (**E**,**F**). Note: AQP1_P: macrophages with positive AQP1 expression; AQP1_N: macrophages with negative AQP1 expression.

reversed this effect (Fig. 6A–D). Furthermore, immunofluorescence analysis and flow cytometry were used to assess macrophage phagocytosis. The findings indicated that the absence of AQP1 abolished the LPS-induced increase in macrophage phagocytosis (Fig. 6E–G). These results suggest that LPS promotes macrophage migration and increases phagocytosis via AQP1.

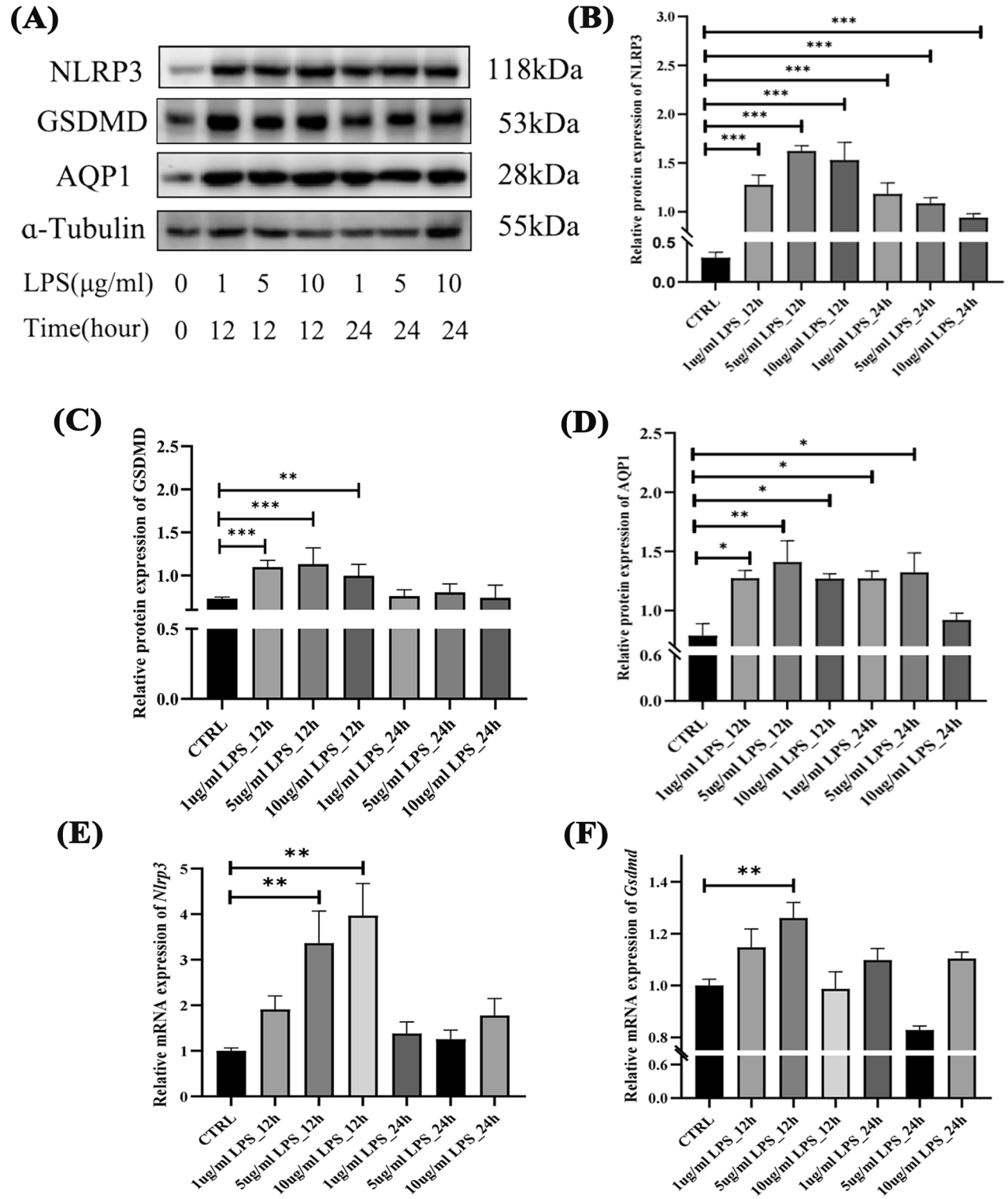

Figure 3. Cell polarization model induced by different concentrations of LPS. (**A**) Representative western blots of NLRP3, GSDMD, AQP1 and α-Tubulin. Effects of exposure to different concentrations of LPS for different times on the expression of NLRP3 (**B**), GSDMD (**C**) and AQP1 (**D**). Effects of LPS on the mRNA levels of NLRP3 and GSDMD (**E**,**F**). $^{*}P<0.05$, $^{**}P<0.01$, $^{***}P<0.001$.

AQP1 increases the response of macrophages to LPS

To further understand the regulatory impact of the AQP1 protein on macrophage function, transcriptome sequencing was performed on the control group, LPS group, and LPS + AQP1 inhibitor group. The sequencing

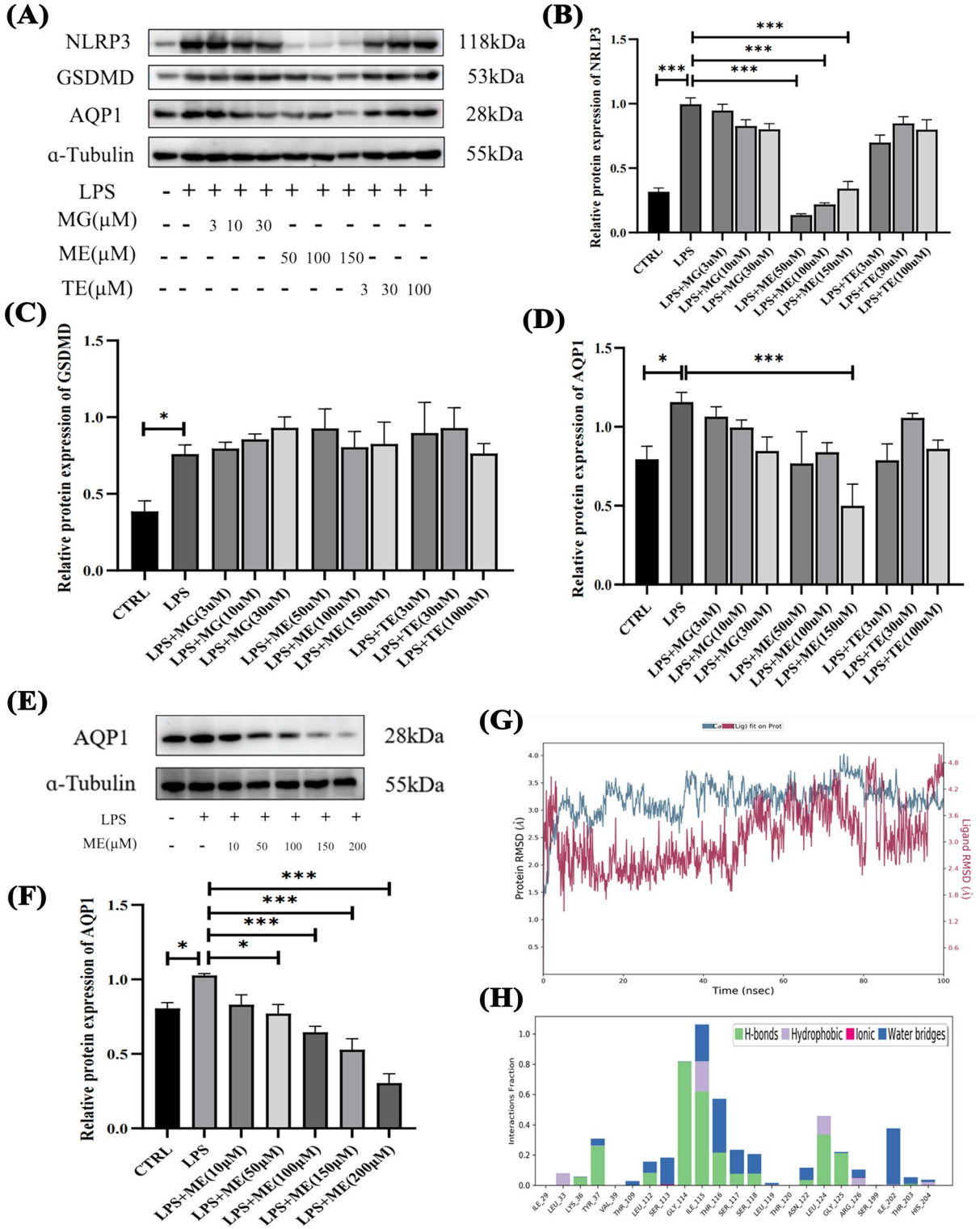

Figure 4. Screening of AQP1 inhibitors. (**A**) Representative western blots of NLRP3, GSDMD, AQP1 and α-Tubulin. The effects of MG132, mercuric chloride and TEA on the protein expression of NLRP3, GSDMD and AQP1 (**B**–**D**). (**E**) Representative western blots of AQP1 and α-Tubulin. The inhibitory effect of different concentrations of mercuric chloride on the AQP1 protein (**F**). The stable binding of mercuric chloride to the AQP1 protein (**G**) and its strong interaction (**H**). *CRTL* Control, *ME* Merbromin, *MG* MG132, *TE* Tetraethylammon. $^{*}P<0.05$, $^{**}P<0.01$, $^{***}P<0.001$.

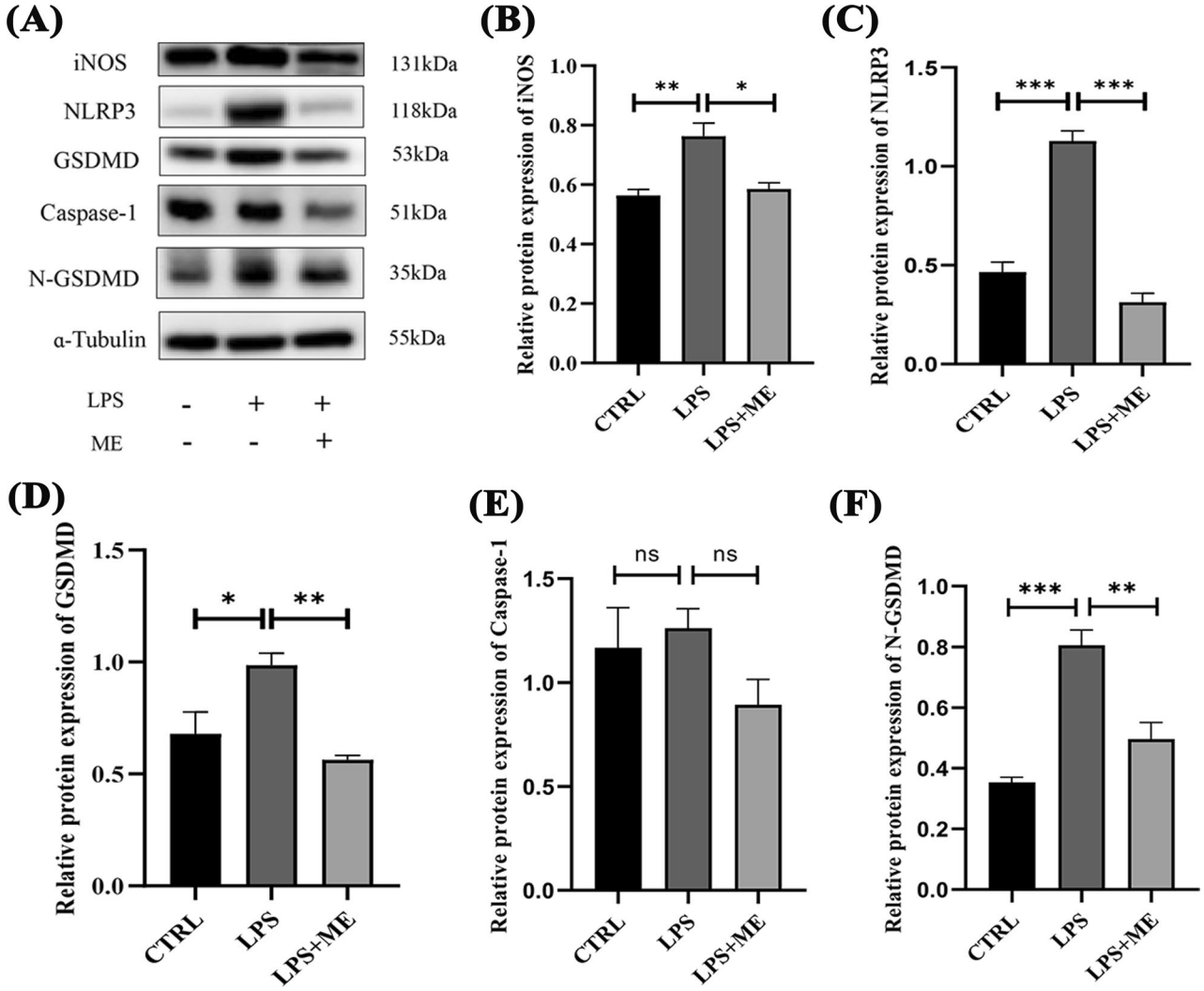

Figure 5. The AQP1 protein is related to LPS-induced macrophage polarization and pyroptosis. (**A**) Representative western blots of iNOS, NLRP3, GSDMD and α-Tubulin. An AQP1 protein inhibitor reduced the degree of M1 polarization (**B**) and pyroptosis (**C**,**D**) induced by LPS. *CRTL* Control, *ME* Merbromin. $^{*}P<0.05$, $^{**}P<0.01$, $^{***}P<0.001$.

data were standardized to ensure balanced and comparable data (Fig. S2A). By using three dimensionality reduction clustering methods, it was observed that the intragroup variability was low, and the differences between the groups were substantial (Fig. S2B–D). Compared to that in the control group, LPS increased the expression of chemokines (Cxcl2 and Cxcl3) and pyroptosis-related molecules (Il-1β) in macrophages, promoting their polarization toward the M1 phenotype (Nos2 and Il-1α) (Fig. 7A). Conversely, the AQP1 inhibitor notably reduced the expression of Il-1β and the degree of M1 polarization (NOS2 and Il-1α) induced by LPS (Fig. 7B). Cross-referencing the opposing gene expression patterns induced by LPS and AQP1 inhibitors revealed that AQP1 inhibitors attenuated the LPS-induced upregulation of 666 genes and reversed the LPS-induced downregulation of 532 genes (Fig. 7C). Pathway analysis of these DEGs indicated that AQP1 inhibitors decreased signaling pathways related to cytokines, NFκB, Toll-like receptors, and chemokines (Fig. 7D). The absence of AQP1 decreased cellular responsiveness to LPS and viruses (Fig. 7E).

AQP1 deficiency reduces the response of macrophages to LPS by reducing the production of chemokines

To further determine key molecules associated with genes that are affect by AQP1 deficiency, a protein−protein interaction network was constructed for the DEGs, and two key modules were identified using MCODE (Fig. S3A,B). Both modules were associated with the cell response to LPS and macrophage chemotaxis (Fig. S3C,D). By using six hub gene screening algorithms, chemokines (Ccl2, Ccl3, and Ccl4) and molecules related to pyroptosis (Il-1β) were shown to play pivotal roles (Fig. S4A–F). Intersection analysis revealed 19 genes that were identified as hub genes by all six algorithms (Fig. 8A) and were associated with chemokine-mediated signals and LPS reactivity (Fig. 8B). Visualization of the expression levels of the hub genes in the three groups showed that AQP1 inhibitors reduced the LPS-induced increase in the expression of these hub genes (Fig. 8C).

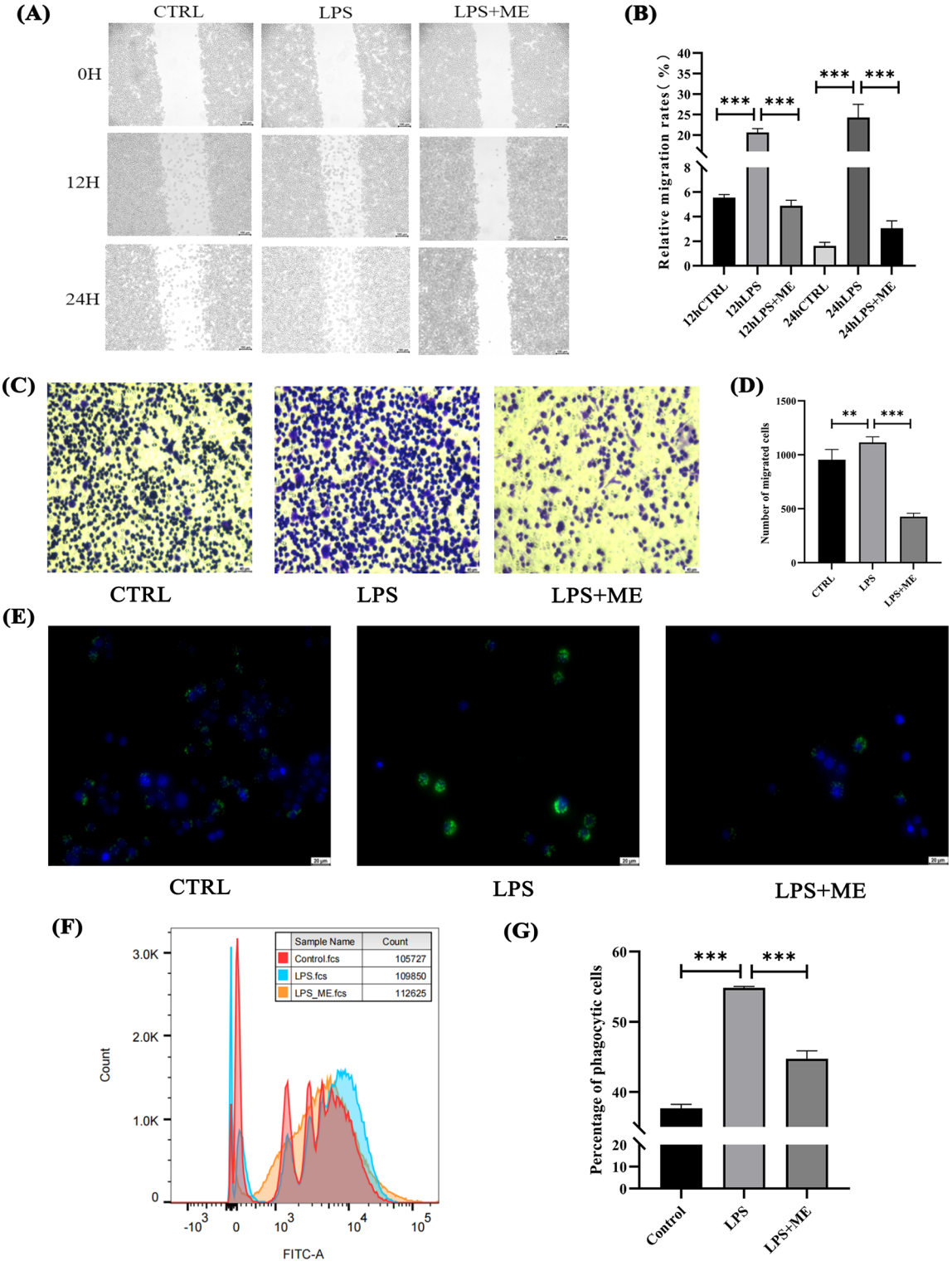

Figure 6. AQP1 protein deficiency reduces LPS-induced macrophage migration and phagocytosis. An AQP1 protein inhibitor reduced the macrophage migration rate (**A**,**B**) and the number of migrating cells (**C**,**D**) induced by LPS. Moreover, the AQP1 protein inhibitor reduced the number (**E**) and proportion (**F**,**G**) of phagocytic macrophages. *CRTL* Control, *ME* Merbromin. *$P<0.05$, **$P<0.01$, ***$P<0.001$.

To clarify the relationship between AQP1 and pyroptosis, the overlap of DEGs and pyroptosis markers was examined. NLRP3 and IL-1β were significantly increased in the LPS group, and the AQP1 inhibitor effectively

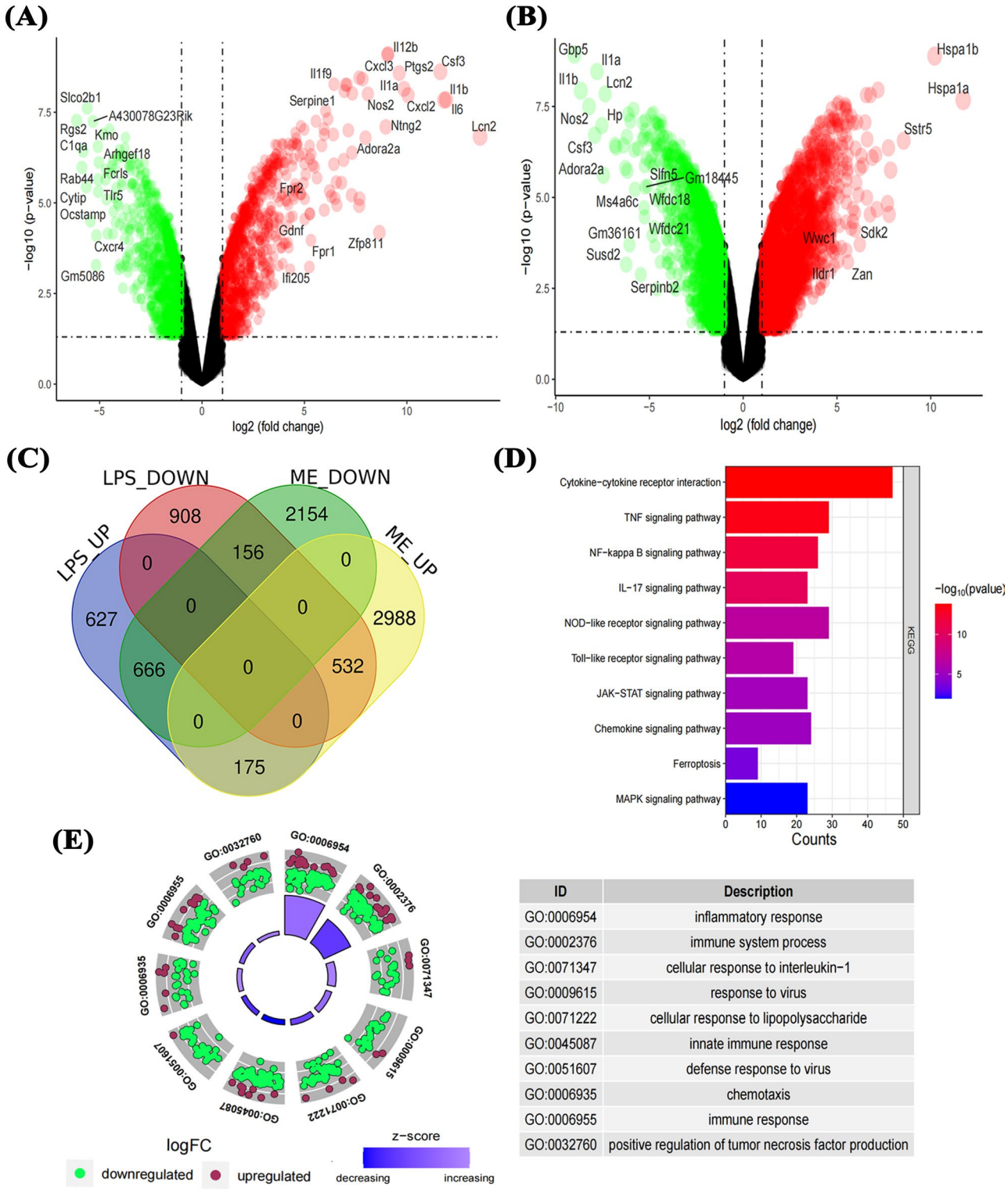

ID	Description
GO:0006954	inflammatory response
GO:0002376	immune system process
GO:0071347	cellular response to interleukin−1
GO:0009615	response to virus
GO:0071222	cellular response to lipopolysaccharide
GO:0045087	innate immune response
GO:0051607	defense response to virus
GO:0006935	chemotaxis
GO:0006955	immune response
GO:0032760	positive regulation of tumor necrosis factor production

Figure 7. AQP1 protein inhibition reduces the reactivity of macrophages to LPS. Volcano map of DEGs in the LPS group (**A**), volcano map of DEGs in the AQP1 inhibitor group (**B**), Venn diagram of DEGs (**C**), KEGG pathway analysis of DEGs (**D**), and GO enrichment analysis of DEGs (**E**) compared with those in the control group. In the Volcano map, the horizontal axis is the logarithmic value of the difference multiple, and the vertical axis is the logarithm of the P value.

mitigated this effect (Fig. S4G–I). Correlation analysis of gene expression indicated a strong correlation between pyroptosis-related genes and hub genes (Fig. 8D).

Verification of chemokines and pyroptosis molecules related to AQP1

Cell experiments revealed that the mRNA levels of chemokines (Ccl2, Ccl3, Ccl4, and Cxcl10) were significantly upregulated in the LPS group, and this effect could be reversed by AQP1 inhibitors (Fig. 9A–D). Cd40, which is a proinflammatory molecule in macrophages, was highly expressed in the LPS group, and the absence of AQP1 significantly mitigated this effect (Fig. 9E). Furthermore, the expression of Icam1 and Il-1α, which play roles in regulating macrophage polarization, decreased in the presence of AQP1 inhibitors (Fig. 9F,G). Additionally, the lack of AQP1 decreased the mRNA expression levels of the pyroptosis-related molecules Il-1β and Nlrp3 (Fig. 9H,I). In addition, enzyme-linked immunosorbent assay showed that AQP1 deficiency reduced the secretion of macrophage chemokine CCL4 (Fig. 9J).

Discussion

Acute lower respiratory tract infections often result in ALI, which is attributed to alveolar epithelial cell dysfunction due to excessive immune cell activation and leads to lung hypoxia[18]. Numerous studies have demonstrated that acute infections can induce macrophage polarization to the M1 phenotype[19], which was confirmed in our investigation. We observed that in patients with severe COVID-19, alveolar macrophages proliferated abnormally and had abnormal activity, such as increased cytokine production and cell migration. The use of M1 polarization markers (TLR2, TLR4 and CD86) to characterize macrophages revealed that severe infection caused macrophages to polarize to the M1 phenotype, which could lead to ALI in patients. Moreover, according to the proportion and enrichment analysis of different macrophage populations in the two groups, M1 macrophage polarization

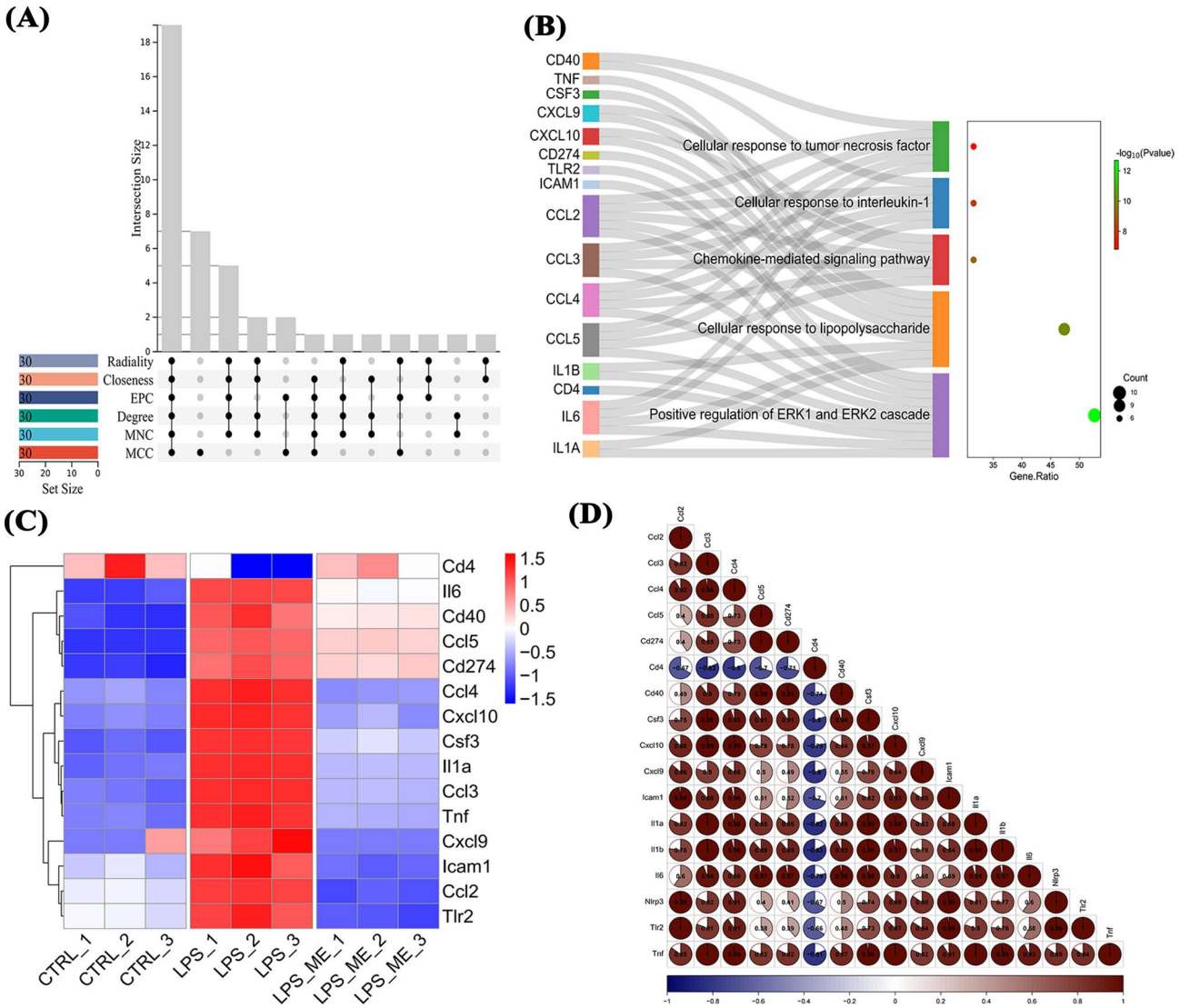

Figure 8. There was a positive correlation between the hub genes and the expression of pyroptosis-related genes. Six algorithms were used to identify the hub genes of DEGs (**A**), functional enrichment analysis of hub genes (**B**) and expression patterns in the different groups (**C**), and the correlation between pyroptosis-related genes NLRP3 and IL-1β and hub genes (**D**).

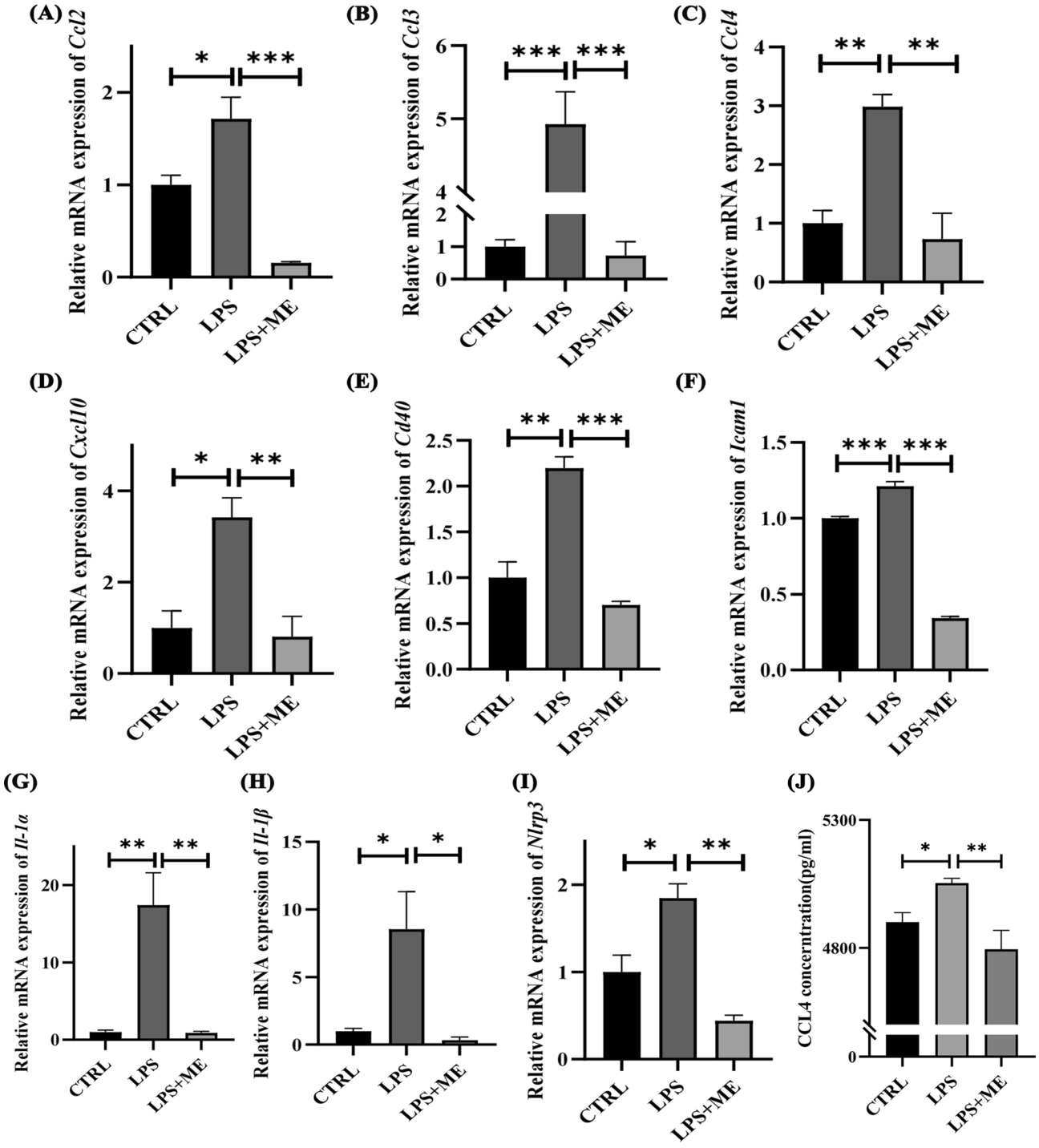

Figure 9. Verification of the expression of hub genes related to pyroptosis. The mRNA expression levels of chemokines (Ccl2, Ccl3, Ccl4, Cxcl10) (**A**–**D**) and the expression levels of Cd40, Icam1, Il-1α, Il-1β and Nlrp3 were detected (**E**–**I**). Expression level of CCL4 protein in different groups (**J**). *CRTL* Control, *ME* Merbromin. $^{*}P<0.05$, $^{**}P<0.01$, $^{***}P<0.001$.

(involving Toll-like receptors and LPS-mediated signaling pathways) occurred in patients with severe COVID-19. These results indicate that infection-induced ALI leads to macrophage polarization toward the M1 phenotype. Interestingly, macrophages that were positive for AQP1 expressed more M1 polarization markers. Moreover, when macrophages expressing AQP1 and M1 polarization markers were compared, we found that their biological functions were surprisingly consistent. Additionally, the increased expression of AQP1 correlated with M1 macrophage polarization and the coexpression of AQP1 and M1 markers in macrophages. Notably, the AQP1 inhibitor significantly inhibited macrophage polarization to the M1 phenotype. This finding suggested that the AQP1 protein could promote M1 macrophage polarization in COVID-19 patients, which was validated in RAW264.7 cells[20].

Previous studies have linked M1 macrophage polarization to pyroptosis[21]. Activation of the NLRP3 inflammasome induces acute kidney injury by triggering downstream inflammatory cytokines and leading to pyroptosis[22]. Similarly, inhibiting the pyroptosis-related proteins NLRP3/GSDMD in macrophages can alleviate ALI by reducing cytokine production[23]. Following viral infection, the increased expression of chemokines and cytokines during M1 macrophage polarization can lead to pyroptosis[24]. Single-cell analysis revealed that M1 macrophage polarization was accompanied by the formation of inflammatory bodies containing NLRP3, and macrophages expressing AQP1 exhibited high expression of molecules related to pyroptosis. In addition, in the M1 macrophage polarization model, both AQP1 and pyroptosis markers were activated by LPS in a dose-dependent manner. The AQP1 inhibitor significantly reduced LPS-induced pyroptosis related non-classical way and Increased chemotaxis. These findings suggest that AQP1 is involved in pyroptosis and can serve as a therapeutic target for regulating pyroptosis and alleviating ALI.

Macrophages play crucial roles in phagocytosis, migration, and antigen presentation. In various tissue injuries, an excessive increase in macrophage phagocytosis has been reported to impair the functionality of surrounding cells[25]. This study revealed a significant increase in antigen processing and presentation, phagocytosis, and migration by macrophages after viral infection, which was consistent with findings in other reports[26]. Similarly, the phagocytic function of M1 macrophages in COVID-19 patients was increased, suggesting that abnormal macrophage function contributes to the onset of ALI. Concurrently, a study revealed that during acute infection, macrophages expressing AQP1 exhibited antigen presentation functions and increased migration (chemokine signaling pathway). The results of transcriptomic analysis and cell experiments showed that a lack of AQP1 could inhibit the migration of macrophages by affecting a variety of chemokines (Ccl2, Ccl3, Ccl4, and Cxcl10), which was confirmed by scratch and transwell tests. Regarding macrophage phagocytosis, immunofluorescence analysis of fluorescent microspheres and flow cytometry indicated that the AQP1 inhibitor effectively mitigated the increase in macrophage phagocytosis induced by LPS. In summary, these results indicate that AQP1 is involved in the abnormal functions of macrophages induced by acute infection and can serve as a therapeutic target for regulating macrophage function in ALI.

Conclusions

This study identified a critical pathological role of AQP1. Specifically, AQP1 could promote the LPS-induced polarization and pyroptosis in M1 macrophages and was closely associated with macrophage phagocytosis and migration. These effects primarily involved the regulation of chemokines and cytokine production. These findings underscore the significance of AQP1 in influencing the diverse functions of macrophages in response to inflammatory stimuli, providing valuable insights into potential therapeutic targets for conditions such as ALI.

Data availability

Single cell data GSE171524 and GSE171668 can be obtained free of charge in GEO database (https://www.ncbi.nlm.nih.gov/geo/), and transcriptome sequencing data can be obtained from the correspondent for reasonable reasons.

Received: 8 January 2024; Accepted: 29 July 2024
Published online: 10 August 2024

References

1. Niederman, M. S. & Torres, A. Respiratory infections. *Eur. Respir. Rev.* **31**(166), 220150. https://doi.org/10.1183/16000617.0150-2022 (2022).
2. Amit, S. *et al.* Postvaccination COVID-19 among healthcare workers, Israel. *Emerg. Infect. Dis.* **27**(4), 1220–1222. https://doi.org/10.3201/eid2704.210016 (2021).
3. Clementi, N. *et al.* Viral respiratory pathogens and lung injury. *Clin. Microbiol. Rev.* **34**(3), e00103-20. https://doi.org/10.1128/CMR.00103-20 (2021).
4. Feng, J. *et al.* Novel insights into the pathogenesis of virus-induced ARDS: Review on the central role of the epithelial–endothelial barrier. *Expert Rev. Clin. Immunol.* **17**(9), 991–1001. https://doi.org/10.1080/1744666X.2021.1951233 (2021).
5. Guo, Y. *et al.* Up-regulated CD38 by daphnetin alleviates lipopolysaccharide-induced lung injury via inhibiting MAPK/NF-κB/NLRP3 pathway. *Cell Commun. Signal.* **21**(1), 66. https://doi.org/10.1186/s12964-023-01041-3 (2023).
6. Zhang, Y. Z., Zeb, A. & Cheng, L. F. Exploring the molecular mechanism of hepatitis virus inducing hepatocellular carcinoma by microarray data and immune infiltrates analysis. *Front. Immunol.* **13**, 1032819. https://doi.org/10.3389/fimmu.2022.1032819 (2022).
7. Chen, X. *et al.* Macrophage polarization and its role in the pathogenesis of acute lung injury/acute respiratory distress syndrome. *Inflamm. Res.* **69**(9), 883–895. https://doi.org/10.1007/s00011-020-01378-2 (2020).
8. Wang, Q. *et al.* Aquaporin-1 inhibition exacerbates ischemia-reperfusion-induced lung injury in mouse. *Am. J. Med. Sci.* **365**(1), 84–92. https://doi.org/10.1016/j.amjms.2022.08.017 (2023).
9. Kang, J. Y. *et al.* Melatonin attenuates LPS-induced pyroptosis in acute lung injury by inhibiting NLRP3-GSDMD pathway via activating Nrf2/HO-1 signaling axis. *Int. Immunopharmacol.* **109**, 108782. https://doi.org/10.1016/j.intimp.2022.108782 (2022).
10. Melms, J. C. *et al.* A molecular single-cell lung atlas of lethal COVID-19. *Nature* **595**(7865), 114–119. https://doi.org/10.1038/s41586-021-03569-1 (2021).
11. Delorey, T. M. *et al.* COVID-19 tissue atlases reveal SARS-CoV-2 pathology and cellular targets. *Nature* **595**(7865), 107–113. https://doi.org/10.1038/s41586-021-03570-8 (2021).
12. Hao, Y. *et al.* Dictionary learning for integrative, multimodal and scalable single-cell analysis. *Nat. Biotechnol.* https://doi.org/10.1038/s41587-023-01767-y (2023).
13. McDavid, A. *et al.* Data exploration, quality control and testing in single-cell qPCR-based gene expression experiments. *Bioinformatics* **29**(4), 461–467. https://doi.org/10.1093/bioinformatics/bts714 (2013).
14. Ritchie, M. E. *et al.* limma powers differential expression analyses for RNA-sequencing and microarray studies. *Nucleic Acids Res.* **43**(7), e47. https://doi.org/10.1093/nar/gkv007 (2015).
15. Wu, T. *et al.* clusterProfiler 40: A universal enrichment tool for interpreting omics data. *Innovation* **2**(3), 100141. https://doi.org/10.1016/j.xinn.2021.100141 (2021).

16. Szklarczyk, D. *et al.* The STRING database in 2021: Customizable protein-protein networks, and functional characterization of user-uploaded gene/measurement sets. *Nucleic Acids Res.* **49**(D1), D605–D612. https://doi.org/10.1093/nar/gkaa1074 (2021).
17. Guo, A. *et al.* Identification of Hub genes and pathways in a rat model of renal ischemia-reperfusion injury using bioinformatics analysis of the Gene Expression Omnibus (GEO) dataset and integration of gene expression profiles. *Med. Sci. Monit.* **25**, 8403–8411. https://doi.org/10.12659/MSM.920364 (2019).
18. Dinnon, K. H. 3rd. *et al.* SARS-CoV-2 infection produces chronic pulmonary epithelial and immune cell dysfunction with fibrosis in mice. *Sci. Transl. Med.* **14**(664), eabo5070. https://doi.org/10.1126/scitranslmed.abo5070 (2022).
19. Wang, Z. & Wang, Z. The role of macrophages polarization in sepsis-induced acute lung injury. *Front. Immunol.* **14**, 1209438. https://doi.org/10.3389/fimmu.2023.1209438 (2023).
20. Lv, W. *et al.* Aquaporin 1 facilitates ferroptosis, M1 polarization, mitochondrial dysfunction, and autophagy damage on lipopolysaccharide-induced macrophage through down-regulation of P53 signaling pathway. *DNA Cell Biol.* **42**(8), 456–480. https://doi.org/10.1089/dna.2023.0016 (2023).
21. Li, N. *et al.* Myoglobin promotes macrophage polarization to M1 type and pyroptosis via the RIG-I/Caspase1/GSDMD signaling pathway in CS-AKI. *Cell Death Discov.* **8**(1), 90. https://doi.org/10.1038/s41420-022-00894-w (2022).
22. Li, N. *et al.* Pathway network of pyroptosis and its potential inhibitors in acute kidney injury. *Pharmacol. Res.* **175**, 106033. https://doi.org/10.1016/j.phrs.2021.106033 (2022).
23. Ding, P. *et al.* Fibroblast growth factor 21 attenuates ventilator-induced lung injury by inhibiting the NLRP3/caspase-1/GSDMD pyroptotic pathway. *Crit. Care* **27**(1), 196. https://doi.org/10.1186/s13054-023-04488-5 (2023).
24. Yan, J. *et al.* CCR5 activation promotes NLRP1-dependent neuronal pyroptosis via CCR5/PKA/CREB pathway after intracerebral hemorrhage. *Stroke* **52**(12), 4021–4032. https://doi.org/10.1161/STROKEAHA.120.033285 (2021).
25. Hill, C. E. A view from the ending: Axonal dieback and regeneration following SCI. *Neurosci. Lett.* **23**(652), 11–24. https://doi.org/10.1016/j.neulet.2016.11.002 (2017).
26. Sefik, E. *et al.* Inflammasome activation in infected macrophages drives COVID-19 pathology. *Nature* **606**(7914), 585–593. https://doi.org/10.1038/s41586-022-04802-1 (2022).

Author contributions
The research design was completed by Wen Zhuman and Ablimit Abduxukur, and Wen Zhuman was responsible for data analysis and cell experiment.

Funding
The research is supported by the National Natural Science Foundation of China (No. 32060158).

Competing interests
The authors declare no competing interests.

Additional information
Supplementary Information The online version contains supplementary material available at https://doi.org/10.1038/s41598-024-68899-2.

Correspondence and requests for materials should be addressed to A.A.

Reprints and permissions information is available at www.nature.com/reprints.

Publisher's note Springer Nature remains neutral with regard to jurisdictional claims in published maps and institutional affiliations.